ADVANCED HEALTHCARE MATERIALS
www.advhealthmat.de

Synchronized Ratiometric Codelivery of Metformin and Topotecan through Engineered Nanocarrier Facilitates In Vivo Synergistic Precision Levels at Tumor Site

*Venkatesh Teja Banala, Shweta Sharma, Puja Barnwal, Sandeep Urandur, Ravi P. Shukla, Naseer Ahmad, Naresh Mittapelly, Gitu Pandey, Monika Dwivedi, Navodayam Kalleti, Kalyan Mitra, Srikanta Kumar Rath, Ritu Trivedi, and Prabhat Ranjan Mishra**

The combination of metabolic modulators with chemotherapy holds vast promise for effective inhibition of tumor progression and invasion. Herein, a ratiometric codelivery platform is developed for metformin (MET), a known metabolic modulator and topotecan (TPT), a chemotherapeutic drug, by engineering lipid bilayer–camouflaged mesoporous silica nanoparticles (LB-MSNs). In an attempt to deliver and maintain high tumor site concentrations of MET and TPT, a novel ion pairing–assisted loading procedure is developed using pamoic acid (PA) as an in situ trapping agent. PA, a hydrophobic counterion, increases the hydrophobicity of MET and TPT and facilitates MSNs with exceptionally high payload capacity (>40 and 32 wt%, respectively) and controlled release profile. Further, the synergy between MET and TPT determined by a modeling approach helps to afford synchronized delivery of both the drugs. Coloaded MET and TPT LB-MSNs present synergistic cytotoxicity against MDA-MB-231/4T1 cells and effectively promote apoptosis via mitochondrial membrane depolarization and cell cycle arrest. Extended pharmacokinetic profiles in preclinical models with fourfold to sevenfold longer circulation half-life and 7.5–100 times higher tumor site concentrations correspond to a significant increase in pharmacodynamic efficacy. Taken together, the developed codelivery approach effectively addresses the challenges in the chemotherapeutic efficacy of MET and TPT collectively.

1. Introduction

Conceding to the shortcomings of contemporary management stratagems, breast cancer exults as one of the most frequent and fatal malignancies among women globally. Progressively more failures of surgical resection, radiotherapy, also hormone therapy, owing to the desensitization of receptors, had raised disquieting ultimatum. The clinical benefits of hormone therapy are limited due to the common issues like drug resistance, dose limited toxicity, and harsh tumor microenvironment that hinder the drug penetration and efficacy.[1] Thus, growing obligation in terms of complexity in treatment manifests the inception of hormone refractory breast cancer. Due to the physiological complexity of the tumor, monotherapy strategies are found to be not effective with more relapse rates which led to an interest in combination chemotherapy regimens, referring to the simultaneous administration of two or more drugs for achieving long-term prognosis with less unwanted side effects.[2] Unlike monotherapy, combination chemotherapies may cause synergistic response, maximize the therapeutic effect, and overcome drug resistance by modulating different signaling pathways in cancer cells. With the increase in understanding of molecular pathways, tumor microenvironment, and host–tumor interactions, new combination therapies are continuously evolving with new paradigms.[2b,3] Combination therapy with drugs that enable

V. T. Banala, Dr. S. Sharma, P. Barnwal, S. Urandur, R. P. Shukla, N. Mittapelly, G. Pandey, Dr. M. Dwivedi, Dr. P. R. Mishra
Division of Pharmaceutics and Pharmacokinetics
CSIR–Central Drug Research Institute
Lucknow 226031, India
E-mail: prabhat_mishra@cdri.res.in, mishrapr@hotmail.com
N. Ahmad, Dr. R. Trivedi
Division of Endocrinology
CSIR–Central Drug Research Institute
Lucknow 226031, India
N. Kalleti, Dr. S. K. Rath
Division of Toxicology
CSIR–Central Drug Research Institute
Lucknow 226031, India
Dr. K. Mitra
Electron Microscopy Division
CSIR–Central Drug Research Institute
Lucknow 226031, India

DOI: 10.1002/adhm.201800300

metabolic reprograming is one such approach gaining more clinical prominence in recent years by addressing chemoresistance and safety concerns tangled in standard chemotherapies.[4]

Recent studies have shown that metformin (MET), a common antidiabetic drug and promising anticancer metabolic modulator, demonstrated significant growth inhibition and proapoptotic effects in several cancers, including breast cancer.[5] MET activates 5′ adenosine monophosphate-activated protein kinase (AMPK), inhibits the mammalian target of rapamycin (mTOR), and downregulates excision repair cross-complementation group 1 (ERCC1).[6] Retrospective studies have reported that patients with diabetes receiving MET exhibited decreased cancer incidence and cancer-related mortality.[7] Various early stage clinical trials are presently underway to probe metformin's potential to combat an array of cancers, including colorectal, prostate, endometrial, and breast cancer.[5a] However, clinical progress of MET as a treatment regimen has been constrained by its rapid elimination, high aqueous solubility, and subtherapeutic tumor site concentrations.[8]

Interestingly, several preclinical studies have shown that MET exerts synergistic effects in combination with various classes of chemotherapeutic agents, like hormone modulation, antimetabolite, antibiotics, and drugs that affect structure and function of DNA.[9] Having realized that MET could show synergistic effects in combination with topoisomerase inhibitors,[10] in this study, we explored the combination therapy of MET with topotecan (TPT) against breast cancer. TPT is a semisynthetic analog of camptothecin suppressing DNA replication by inhibiting the nuclear enzyme topoisomerase I. TPT has been licensed to be a second line anticancer agent for small cell lung cancer (SCLC)[11]and ovarian cancer.[12] In addition to its cytotoxic activity against solid tumors, TPT has shown potential activity against metastases from breast cancer[13] and SCLC[14] in numerous clinical reports.

Theoretically, the success of combination chemotherapy in cancer majorly depends on the ratios of individual agents at the tumor site. Accounting to the dissimilar pharmacokinetic profiles of individual drugs, meager penetration, and heterogeneous distribution, the redemption of actual synergistic ratios at the target site confronted issues to realize the ultimate therapeutic effect of the regimen.[15] To mitigate the problems associated with free drug combination therapy, nanoparticles have formulated to coload synergistic drug combinations.[16] Delivery of synergistic drug ratios through nanocarriers provides controlled, temporal, and spatial delivery of multiple cargos, enables drug accumulation in tumor, and releases the drugs at a synchronized rate, thereby, probability of maintenance of intracellular synergistic drug concentrations is possible.[15c,17] But, coencapsulation of multiple drugs with different physicochemical properties in the same nanocarrier and controlling the drug release are always challenging tasks.[18] Appropriate physical- and chemical engineering of the nanoparticles are needed to enable optimal loading of multiple drugs and by imparting adjustable release kinetics to the delivery vehicle commensurate the required concentration–time profile at the site of action.[19]

Herein, we describe the coencapsulation of MET and TPT in a lipid bilayer–coated mesoporous silica nanoparticles (LB-MSNs) with an aim to achieve high payload and controlled release profile. Among candidate nanocarriers, MSNs offers many advantages over polymeric and lipidic delivery systems, such as uniform controlled particle size and shape with high surface area and modifiable surface chemistry which can widely accommodate high payloads of disparate cargos.[20] However, MSNs often require coatings to shield the surface silanol groups that are highly lipophilic and known to promote nonspecific binding and mononuclear phagocytic system (MPS) uptake.[21] In this context, lipid bilayer–coated MSNs have unique attributes which combine the advantages of liposomes with MSNs. To date, several studies reported the effective delivery of multiple classes of drugs and drug combinations using lipid bilayer–supported MSNs with excellent in vitro and in vivo results.[22] Since, MET is a highly water-soluble drug (>300 mg mL^{-1}), conventional polymeric and lipidic nanoparticulate systems fail in achieving reasonable payload efficiency. Our initial trials with PLGA nanoparticle could be able to accommodate less than 5% w/w of MET with rapid release within 8 h (data not shown). Although liposomal system exhibited efficient loading, inherent stability and burst release drawn obscure inferences for the liposomal system.[23] To overcome these challenges, we developed a novel hydrophobic ion trapping–assisted loading of MET and TPT using pamoic acid (PA) as in situ ion trapping agent. The large surface area of MSNs enables to achieve a high payload of both the drugs and in situ ion trapping offers reasonable hydrophobicity to MET, whereas, TPT exhibited protagonist for controlling the release. The in vitro synergy evaluation between MET and TPT using modeling approach is a major highlight of the study, where the derived ratiometric payload of drugs was delivered and evaluated for enhancement of total efficacy of plain drugs in comparison to the mixture of nanoparticles and coloaded nanoparticles. Additionally, pharmacokinetic studies and intratumoral drug concentrations were determined as a measure of maintenance of synergistic drug ratios and local drug bioavailability. The pharmacodynamic capability of the designed approach was evaluated in 4T1 tumor–bearing mouse model. Overall, this work illustrates the example of how to rationally design and coencapsulate highly water-soluble drugs with controlled release, how modifying the drug loading conditions can affect drug coencapsulation and provides insights on designing combination chemotherapy studies for assessing drug synergism in vitro and in vivo.

2. Results and Discussion

2.1. Coencapsulation of MET and TPT in Lipid Bilayer–Coated Mesoporous Silica Nanoparticles Using PA as In Situ Hydrophobic Ion Pairing (HIP) Agent

In this study, we have selected two water-soluble drugs, MET and TPT for the coencapsulation into the MSNs. Here, we took a major challenge to entrap highly water-soluble MET (>300 mg mL^{-1}) into the MSNs with an objective to control the release reasonably for a duration of 24–48 h. To achieve this goal, we have used PA as novel in situ hydrophobic ion trapping agent (HIP) for high drug loading and controlled release. To understand the HIP formation, metformin pamoate (MET-PA) and topotecan pamoate (TPT-PA) salts were synthesized and confirmed with ^{1}H-NMR (see the Supporting Information for a detailed discussion). From the equilibrium solubility experiments, it was clear

that aqueous solubility of HIPs was ≈40-fold and ≈7.7-fold lower for MET-PA and TPT-PA, respectively, in comparison to plain drugs (Figure S1D,F, Supporting Information).

Although HIP formation is confirmed, one major challenge in loading MET is its low permeability across lipid bilayer due to its ionic nature and high pK_a (>12.4.). Based on various reports and evidences stating the ionic transport of drugs, we have performed transwell artificial membrane permeability assay for MET at different temperature and pH conditions.[24] It was observed that the effective permeability of MET was increased from fivefold to 28-fold with an increase in temperature and pH (Figure S2A1, Supporting Information). After understanding the positive effects of pH and temperature on the permeability of MET, we proceed to develop an active loading approach using PA as ion trapping agent. Initially, we have encapsulated MET and TPT individually into LB-MSNs. The passive entrapment of the MET and TPT into the cores of MSNs achieved a loading efficiency of 18 and 15 wt%, respectively. In our preliminary examination, it was found that plain MET-loaded MSNs could not sustain the drug release due to the high aqueous solubility. With an aim to load further high amount of drug with a controlled release, we have developed a novel remote loading technique. To the best of our knowledge, this is the first report of using in situ hydrophobic ion pairing for high drug loading of water-soluble drugs.

To develop remote loading procedure we used PA-loaded LB-MSNs, (PA)LB-MSNs, composed of SoyaPC/cholesterol/1,2-distearoyl-sn-glycero-3-phosphoethanolamine-polyethylene glycol-$_{2000}$ (DSPE-PEG$_{2000}$) at a molar ratio of 7:2.75:0.25 (**Figure 1**A). The (PA)LB-MSNs were incubated in 10 mg mL^{-1} of MET and 1 mg mL^{-1} of TPT drug solutions. The gradient and electrochemical potential across the lipid membrane and other factors like pH and incubation temperature allow the drug to drive inside the MSNs and get entrapped inside the pores as HIP after precipitating with the counterion, PA (Figure 1B). Different loading parameters were employed to achieve efficient loading. For MET, an optimum pH 9 was maintained outside the MSNs. Although MET exists in ionic form, pH 9 was selected to prevent the harsh environment. For TPT, being an amphipathic base pH 7.4 was found sufficient to maintain the gradient for the remote loading into MSNs. Under defined conditions, we able to achieve a maximum loading of ≈40 wt % for MET and ≈32 wt% for the TPT. The coloading was performed under the conditions of MET by which we have achieved around 35 wt% of MET and 10 wt% of TPT. For all the formulations, we have selected an optimum 4 h of incubation time for efficient loading.

Although we have achieved a maximum loading up to 35–40%, we have chosen to load 25% of MET and 0.5% of TPT based on efficient synergy achieved in in vitro modeling studies. To achieve 25/0.5 wt% ratio of loading, we have used 5 mg mL^{-1} of MET and 0.08 mg mL^{-1} of TPT solutions with triethylamine (TEA) as gradient ion for loading.

2.1.1. Physicochemical Characterization of LB-MSNs

Size measurements by DLS technique revealed that the particle size of LB-MSNs was 97.33 ± 5.63 nm, upon loading of PA, the size was slightly increased to 110 ± 8.85 nm. No significant change in size was observed before and after drug loading of MET and TPT with in situ HIP approach (MP)LB-MSNs, (TP) LB-MSNs, and coloaded MSNs, (MP+TP)LB-MSNs. This is again confirmed by the transmission electron microscopy which reveals a uniform intact coating of the lipid bilayer (**Figure 2**A).

Zeta potential measurements of plain MSNs, LB-MSNs, (MP) LB-MSNs, (TP)LB-MSNs, and coloaded (MP+TP)LB-MSNs were shown in Figure 2A. There is a marked difference in zeta potential observed in plain and LB-MSNs which is an indirect confirmation of the intact coating of the lipid bilayer. Drug loading procedures did not affect the zeta potential of the formulations.

To confirm the in situ HIP formation after drug loading, MSNs were evaluated by infrared spectroscopy (Figure 2B). The characteristic peaks at 3466 (O—H stretch), 3166 (N—H stretch), 2927 (N—H stretch), 1640 (C=O stretch), 1507 (C=O stretch), and 1269 cm^{-1} of MET-PA salt were also observed on (MP)LB-MSNs and (MP+TP)LB-MSNs, confirming the formation of HIP inside MSNs. Similarly TPT-PA characteristic peaks 3402 (O—H stretch), 2978 (C—H stretch), 2879 (C—H stretch), 1740 (C=O stretch), 1651 (C=N aromatic stretch), 1590 (C=C aromatic bend), 1506 (C=O stretch), and 1160 cm^{-1} (C—N stretch) were observed in (TP)LB-MSNs and (MP+TP)LB-MSNs. As can be seen clearly, Fourier-transform infrared (FT-IR) spectra of MSNs with PA salts of both MET and TPT closely match with the respective salts (MET-PA and TPT-PA). This confirms the in situ HIP formation between active pharmaceutical ingredient (API) and counterion similar to that of solid salts.

2.1.2. Evaluation of Key Drug Loading Parameters of the Counterion on Drug Loading Efficiency

As a part of the study, we have also evaluated basic parameters such as the type of gradient ion, pH, and temperature that could affect the drug loading efficiency. We have evaluated three gradient ions of PA, sodium, ammonium, and TEA. All the gradient ion concentrations were kept constant at 10×10^{-3} M equimolar concentration of PA throughout the experiment. From the results, it was evident that TEA (42 wt%) was most efficient gradient ion followed by ammonia (32 wt%) and sodium ions (28 wt%) Figure 2C. Apart from this, pH of the outer phase is a critical parameter which affects the gradient required for the influx of drug into MSNs. Both the drugs behaved in a different manner with the pH, since MET is highly ionic in nature, we expected low drug loading into MSNs, but conversely, we observed a better drug loading of MET than TPT, increase in the pH resulting in a slight improvement in loading.

We also considered temperature and duration of incubation on the drug loading. The temperature was found to have a profound effect on drug loading capability for both the drugs. A temperature of 55–60 °C was found to be suitable with an optimum 4 h of incubation time for efficient drug loading (Figure 2C). Increase in drug loading may be due to increased lipid bilayer permeability and higher pore volume at higher temperatures.

2.1.3. In Vitro Drug Release Studies

To evaluate the efficiency of the developed formulation, in vitro drug release studies were performed for (MP)LB-MSNs,

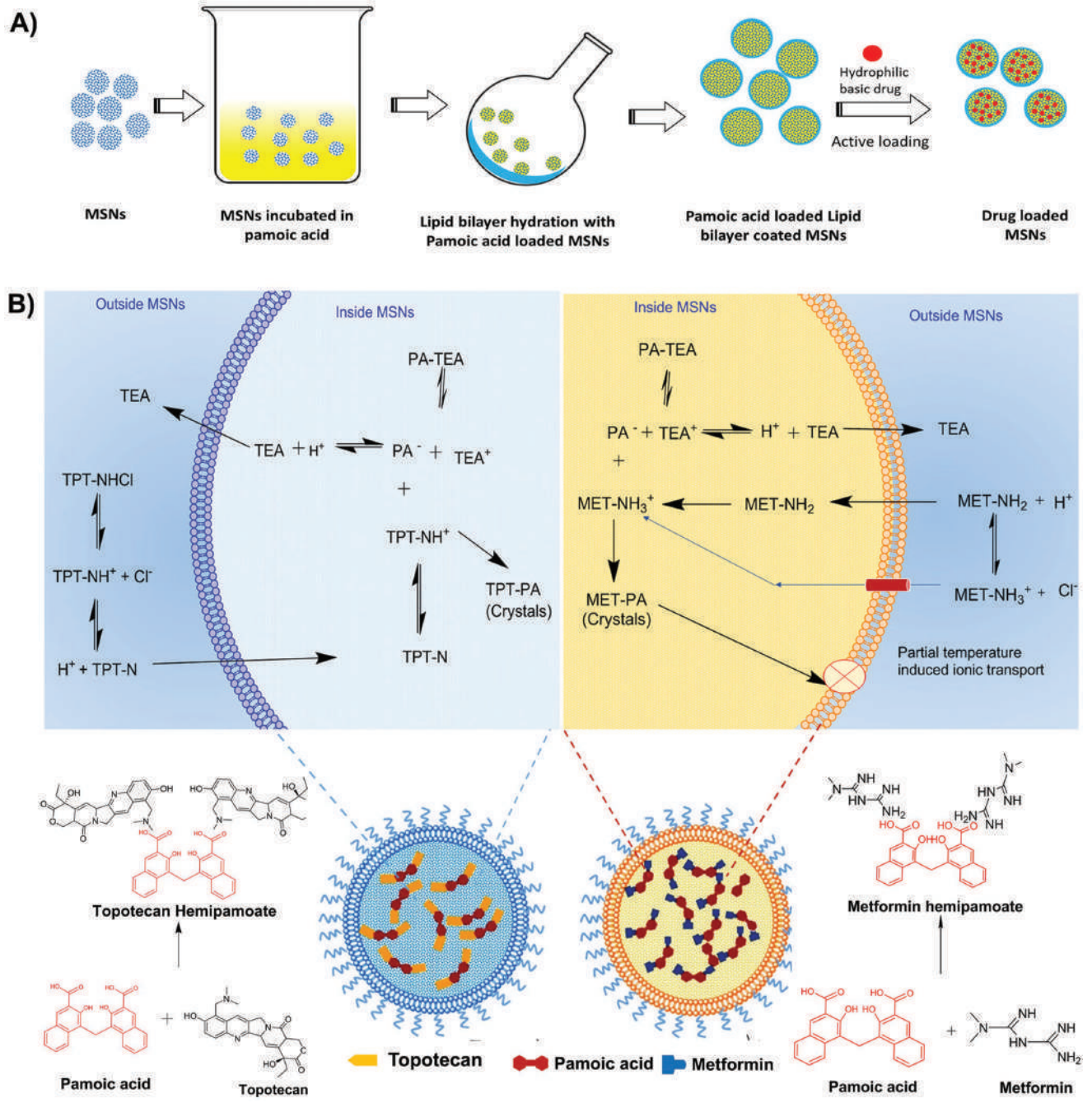

Figure 1. A) Schematics depicting the stepwise preparation of LB-MSNs. B) Mechanistic representation of active loading procedure in PA-loaded LB-MSNs, TEA salt of PA present inside the LB-MSNs allows basic drugs into the MSNs due to gradient difference across the membrane. In case of MET, the higher temperatures partially influence the lipid bilayer permeability. Basic drug after reaching inside MSNs reacts with PA and forms a hydrophobic ion pair (HIP) inside MSN.

(TP)LB-MSNs, and coloaded MSNs with and without trapping agent at two different pH 7.4 and 5.5 to simulate blood and tumor microenvironment, respectively. (MP)LB-MSNs showed sustained release up to 48 h with a cumulative drug release of 95% at pH 5.5 and 86.5% at pH 7.4 (Figure 2D). However, drug release from (TP)LB-MSNs was slower than (MP)LB-MSNs, where 76% and 52% of cumulative TPT release was observed at pH 5.5 and 7.4 within 48 h (Figure 2D). No significant difference in release was observed in the coloaded formulation (MP+TP)LB-MSNs compared to individual drug-loaded formulations. The differential release of MET and TPT from the formulation with trapping agent may be attributed to the difference in hydrophobicities of in situ formed HIPs, MET-PA and TPT-PA, where the solubility of MET-PA (7.4 mg mL^{-1}) was relatively more compared to TPT-PA (0.16 mg mL^{-1}). It was also observed that coloaded formulation without trapping

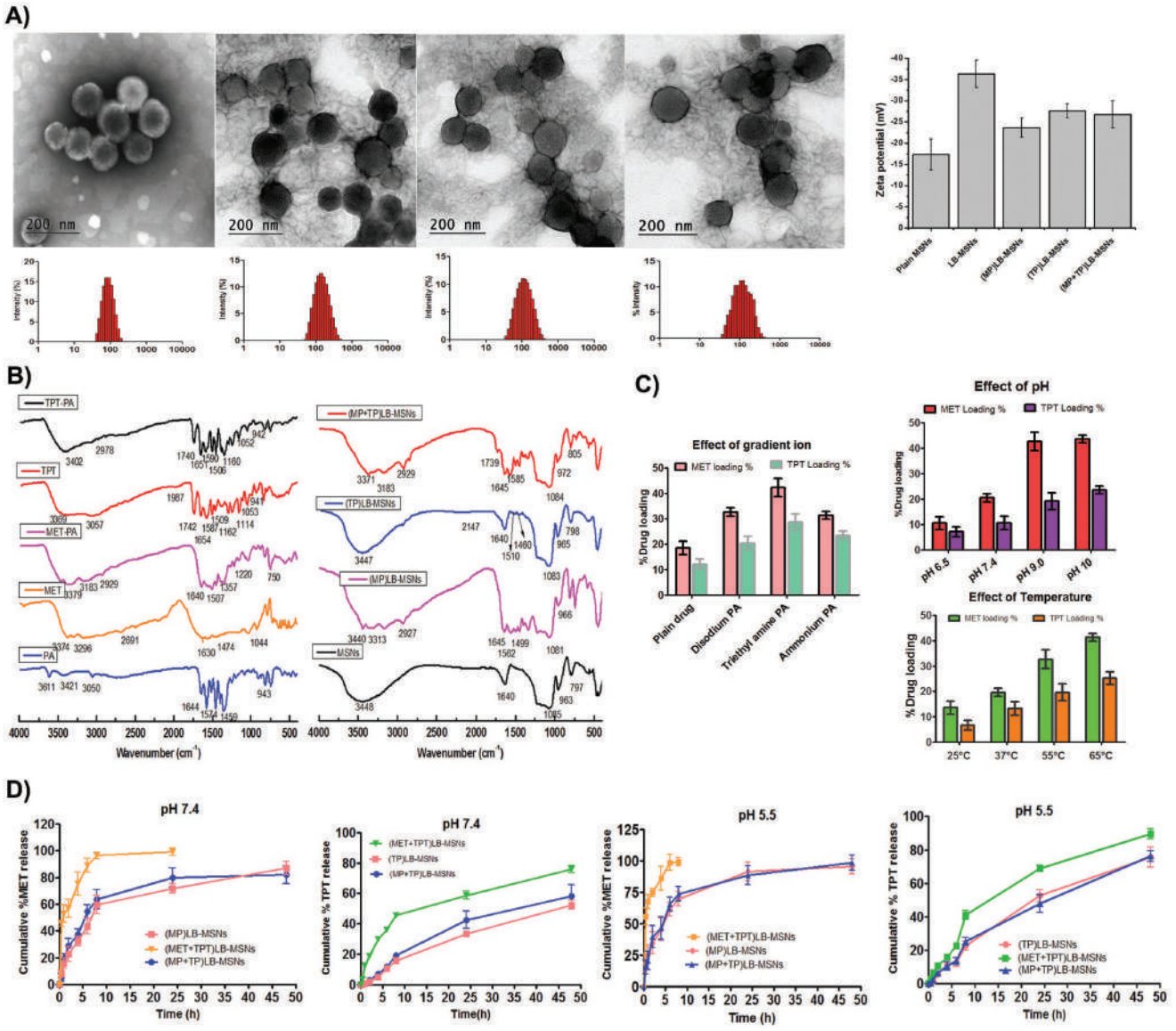

Figure 2. A) Size and polydispersity index (PDI) data of different MSNs, images of transmission electron microscopy (TEM) and dynamic light scattering (DLS) of LB-MSNs, (MP)LB-MSNs, (TP)LB-MSNs, (MP+TP)LB-MSNs (from left to right), and change in zeta potential of different formulations. B) FT-IR of single components (MET, TPT, PA), MET-PA, TPT-PA salts, blank MSNs, and MSNs containing MET, TPT, and PA. C) Various factors affecting the drug loading efficiency; effect of pH, effect of type of gradient ion, and effect of temperature. D) In vitro cumulative percent drug release profiles of MET and TPT from various MSN formulations at pH 7.4 and pH 5.5. All data are expressed as mean ± SD ($n = 3$).

agent, (MET+TPT)LB-MSN was unable to control the release of MET from the MSNs (75% drug release in 4 h at pH 7.4). But, TPT release was comparatively controlled from MSNs without trapping agent (36.6% in 6 h at pH 7.4) which may be due to inherent lipophilic interactions toward silanol groups of MSNs.

The use of LB-MSNs as a delivery vehicle and in situ HIP formation substantially increase the release time of MET which is a major challenge. Using LB-MSNs, Liu et al. reported irinotecan delivery, in which fivefold increase tumor distribution and 11-fold increase in plasma half-life with a controlled in vivo release of more than 48 h were achieved.[25] Similarly, Meng et al. successfully codelivered gemcitabine and paclitaxel in synergistic ratios using lipid bilayer–coated MSNs with a controlled release of water soluble gemcitabine for more than 48 h, in vitro.[26] In comparison to similar delivery systems, present results substantiate its efficacy as a codelivery platform to achieve synergistic tumor site concentrations.

2.2. In Vitro Cell Culture Studies

2.2.1. Identification of Effective Synergy Combinations between MET and TPT Using Mathematical Modeling

To evaluate the combined effects of MET and TPT, 6 × 6 concentration combination experiments were performed in

MDA-MB-231 and 4T1 cell lines using 3-(4,5-dimethylthiazol-2-yl)-2,5-diphenyltetrazolium bromide (MTT) assay after 48 h treatment. We have investigated concentration ranges, $0.01 \times 10^{-3} - 5 \times 10^{-3}$ M of MET and $0.01 \times 10^{-6} - 5 \times 10^{-6}$ M of TPT. After MTT treatment and obtaining the growth inhibition data, we have used COMBENFIT software package to objectively identify the synergistic combinations of MET and TPT. We assessed the region of the synergy of each combination independently with three established mathematical models, such as Bliss, Loewe, and highest single agent (HSA) models.[27] Particulars of these models and their relative advantages can be found in previous publications.[28] From the modeling data, we identified that effective synergy was present with $0.05 \times 10^{-3} - 0.5 \times 10^{-3}$ M of MET and 0.1×10^{-6}–1×10^{-6} M of TPT in both the cell lines (**Figure 3**A and Figure S4A (Supporting Information)). The analysis of single-agent effect reveals, that inhibitory concentration (IC50) (IC50) of MET and TPT was 3.95×10^{-3} M and 1.15×10^{-6} M, respectively, in MDA-MB-231 cell line and 3.59×10^{-3} M and 1.01×10^{-6} M in 4T1 cell line, respectively (Figure 3C and Figure S4C (Supporting Information)).

After identification of the synergy combinations, we tried to analyze the same with the developed formulations. We

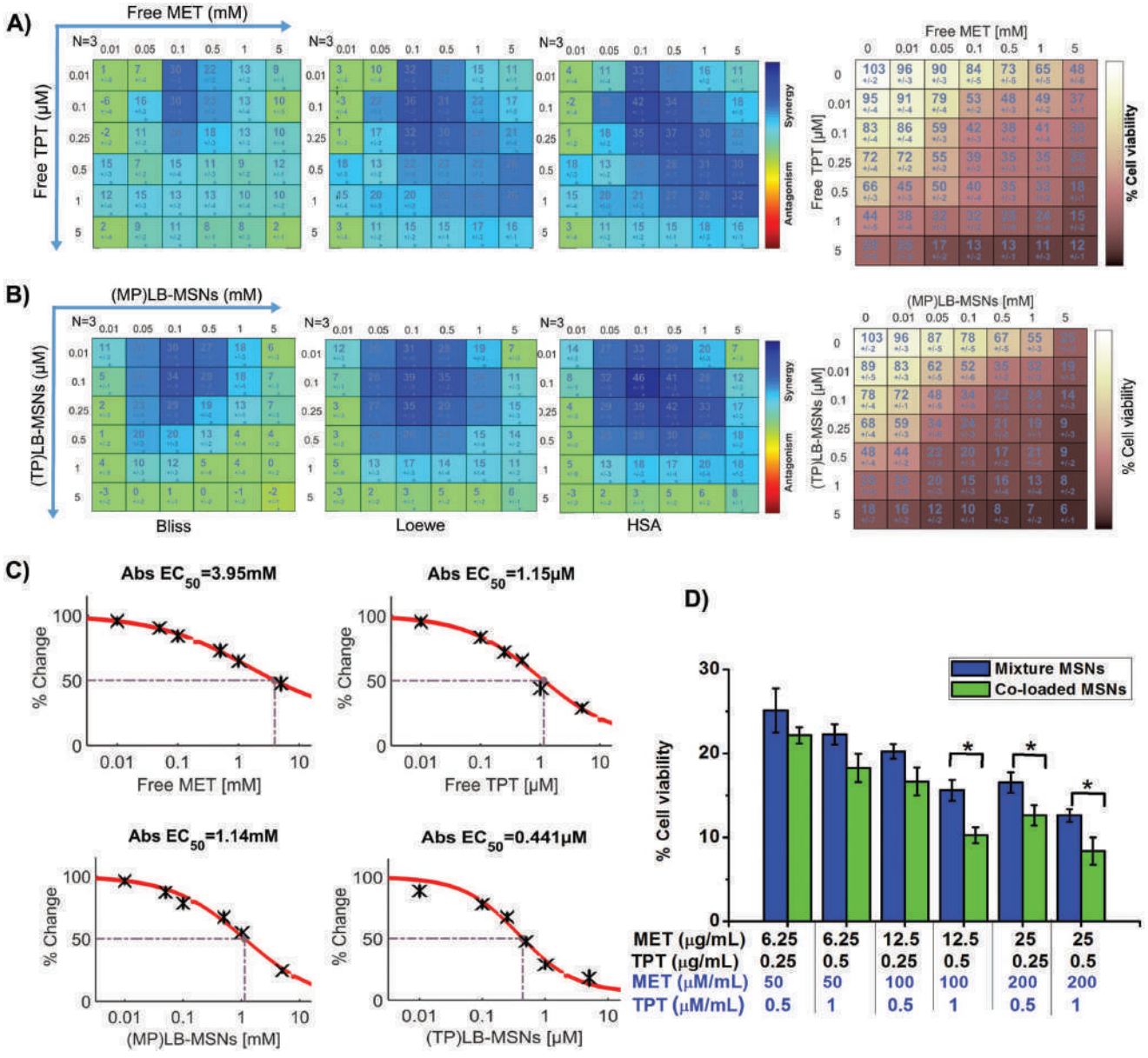

Figure 3. Predicted inhibition data of the three synergy models [Bliss, Loewe, highest single agent (HSA)] in MDA-MB-231 cells treated with A) free MET (*x*-axis) and free TPT (*y*-axis), B) (MP)LB-MSNs and (*x*-axis) and (TP)LB-MSNs (*y*-axis) in 6 × 6 concentration checkerboard format for 48 h using MTT assay. All data are expressed as mean ± SD, $n = 3$, $^{*}p \leq 0.05$; $^{**}p \leq 0.01$; the synergy spots are represented blue in the matrix and experimental data of growth inhibition compared with control are presented. C) Single-agent effect IC50 of the individual drug and drug-loaded LB-MSNs. D) Comparative growth inhibition data of the coloaded and mixture formulations in definite ratios. All data are expressed as mean ± SD, $n = 3$, $^{*}p \leq 0.05$.

repeated the same experiment with a mixture of individual drug-loaded LB-MSNs, i.e., (MP)LB-MSNs and (TP)LB-MSNs in the drug equivalent ratios. After data treatment, we found a good enhancement in the representative synergistic score of the individual models with a significant reduction in the individual IC50 values (Figure 3B and Figure S4B (Supporting Information)). It was found that IC50 of (MP)LB-MSNs and (TP)LB-MSNs was reduced to 1.14×10^{-3} and 0.44×10^{-6} M, 1.33×10^{-3} and 0.40×10^{-6} M in MDA-MB-231 and 4T1 cell lines, respectively (Figure 3C and Figure S4C (Supporting Information)). IC50 of encapsulated drugs were 35–50% lower than free drugs. From the data, it was also clear that synergy was present with 0.05×10^{-3}–1×10^{-3} M of MET and 0.1×10^{-6}–1×10^{-6} M of TPT.

To observe the cytotoxicity of the drug-free MSNs, we carried out the cell viability studies for blank LB-MSNs and (PA) LB-MSNs up to 5 mg mL^{-1} concentration in MDA-MB-231 and 4T1 cell lines. From the results (Figure S3, Supporting Information), it was clear that drug-free LB-MSNs and pamoic acid-loaded LB-MSNs, and (PA)LB-MSNs did not exert cytotoxic effects at the experimental concentrations of in vitro studies.

Based on these modeling data, practical formulation, and dosing aspects, we tried to rationally design the coloaded LB-MSNs. Initially, we have selected six combinations of MET/TPT (50/0.5, 50/1, 100/0.5, 100/1, 200/0.5, and 200/1 of MET/TPT ($\times 10^{-6}$ M)). From the MTT assay, it was observed that coloaded formulations were proven furthermore efficacious compared to a mixture of individual formulations (Figure 3D). Considering the practical loading aspects in MSNs and clinically relevant dosing, we have selected 200/1 (in $\times 10^{-6}$ M) molar ratio of MET/TPT for in vivo studies which meets the practical loading of 25 (wt%) MET and 0.5 (wt%) TPT loading.

2.2.2. Cell Uptake Studies

To evaluate the codelivery efficiency of the LB-MSNs, cellular uptake behavior was monitored in MDA-MB-231 cells using confocal microscopy. To test the hypothesis that the coloaded nanoparticles ensure the deterministic delivery of both cytotoxic drugs versus stochastic distribution in a mixture of nanoparticles, we engineered nanoparticles tagged with fluorescein isothiocyanate (FITC) (green) or rhodamine B, (Red) tracers. MDA-MB-231 cells were incubated with either a combination of FITC-loaded LB-MSNs, (FITC)LB-MSNs, and rhodamine B-loaded LB-MSNs, (RhB)LB-MSNs, or coloaded MSNs, (FITC+RhB)LB-MSNs which contain both the tracers. Interestingly, confocal microscopy revealed that while a large fraction of cells internalizes both the nanoparticles, there was certain cell population that took up either FITC or RhB particles alone (Figure S5, Supporting Information).

2.2.3. Codelivery of MET and TPT Enhances Induction of Cell Cycle Arrest and Apoptosis via Alteration in Mitochondrial Membrane Potential

To further evaluate the intracellular effects of various formulations loaded with MET and TPT alone and in combination, cell cycle analysis, mitochondrial membrane potential, and apoptosis studies were performed using flow cytometric analysis. In cell cycle analysis, the nuclear content of the treated cells was quantified on the basis of propidium iodide (PI) signals and mitochondrial membrane depolarization was measured with the help of JC-1 dye. To quantify the apoptosis, widely used Annexin-V FITC binding–based flow cytometric assay was performed. It is well known that apoptosis occurs by two pathways: the death receptor–mediated and mitochondrial pathways.[29] It is widely studied that mitochondrial depolarization is one of the major pathway involved in the apoptosis induced by MET[30] and TPT.[31] As illustrated in **Figure 4**, the treatment with MET and TPT alone and in combination induced mitochondrial membrane depolarization that leads to cell cycle arrest and subsequently apoptosis. MSNs loaded with MET and TPT, [(MP)LB-MSNs, (TP)LB-MSNs, and (MP+TP)LB-MSNs)] further enhanced the apoptotic effects via mitochondrial membrane depolarization in a synergistic manner. Quantitatively, free MET and TPT induce mitochondrial depolarization in 14.03% and 15.01% cell population, respectively. But, in combination treatment with free drugs slightly enhanced the population which was observed to be antagonistic. Drug-loaded LB-MSNs significantly enhanced the depolarization representing 27.08% and 31.03% of cell population for (MP)LB-MSNs and (TP)LB-MSNs, respectively. In combination treatment, coloaded formulation, (MP+TP)LB-MSNs had shown higher depolarization (54.98%) compared to mixture LB-MSNs (42.25%) and Free MET+TPT (20.81%).

As depicted from the cell cycle analysis data, free MET and (MP)LB-MSNs displayed vivid G1 phase arrest via activation of AMPK through upregulation of p53–$p21^{waf1}$ axis.[32] Whereas free TPT, (TP)LB-MSNs showed prominent G2 phase arrest. Compared to plain TPT (G2-21.89%) (TP)LB-MSNs induced more G2 phase arrest. In combination studies, the effect of MET+TPT showed a pronounced effect compared to individual treatments and it was also observed that MET+TPT combination induced more S phase and G2 phase arrest contrary to G1 phase arrest. Quantitatively, there was more pronounced effects observed in groups of the coloaded formulation (MP+TP) LB-MSNs, (G2-39.84%, S-57.72%), compared to the mixture of drug loaded MSNs (MP)LB-MSNs+(TP)LB-MSNs, (G2-41.5% S-47.46%). In a similar manner subsequent to cell cycle arrest, treatment with coloaded formulation induced more apoptosis compared to the mixture of MSNs loaded with two individual drugs after 48 h of treatment. (MP+TP)LB-MSNs induced 65.52% of apoptosis compared to a mixture of MSNs loaded with individual drugs, 47.94%. This represents that the codelivery of MET and TPT demonstrated collaborative effects on mitochondrial depolarization and cell cycle arrest, resulting in MDA-MB-231 cell apoptosis. This clearly demonstrates that the deterministic delivery of drugs in a single nanoparticle system would be more advantageous compared to a mixture of nanoparticles.

2.3. In Vivo Studies

2.3.1. In Vivo Near Infrared Fluorophore (NIRF) Live Imaging

In order to follow the biodistribution of the LB-MSNs to the tumor site, animals were intravenous (i.v.) injected with

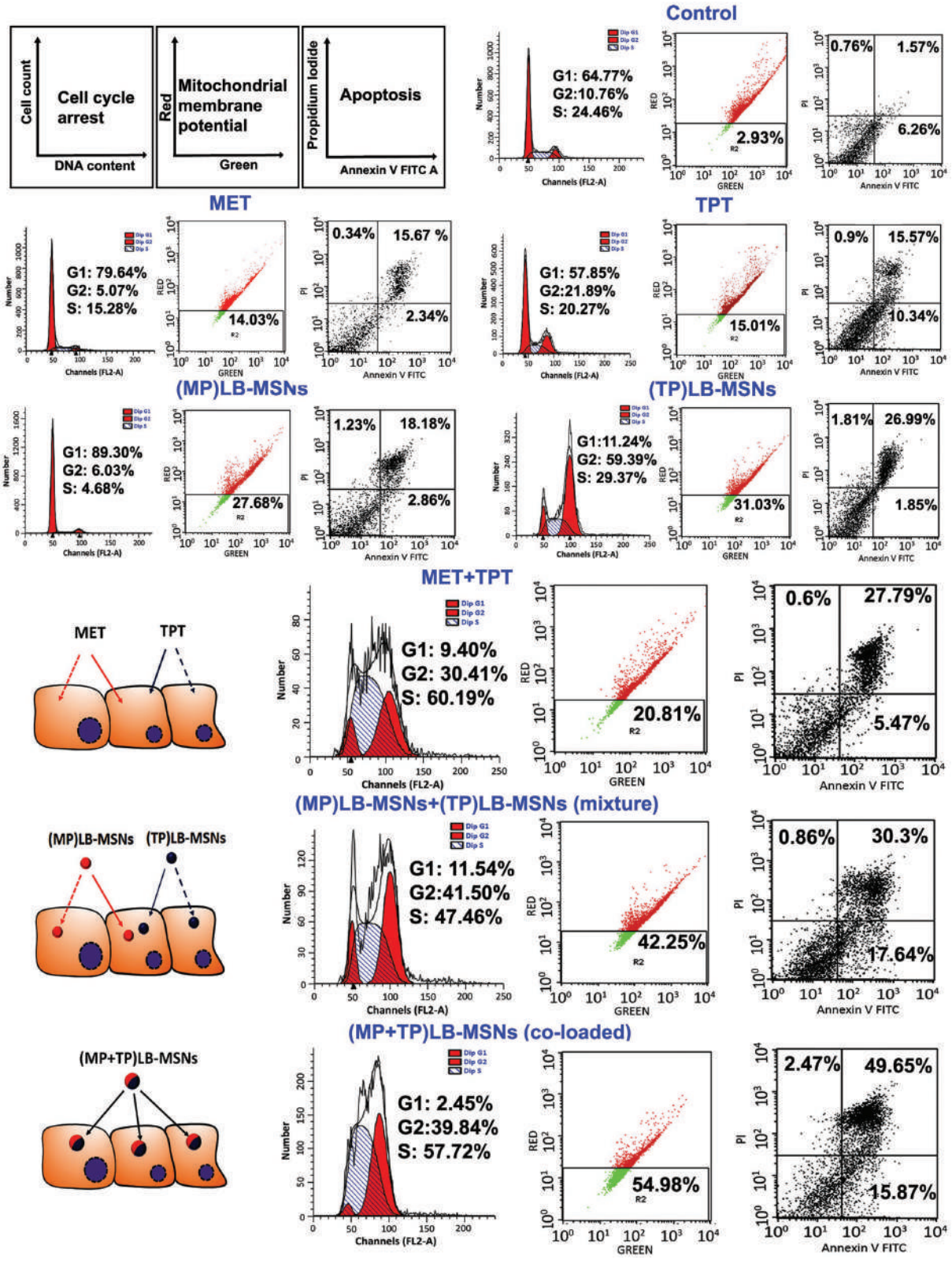

Figure 4. Representative flow cytometry images of cell cycle arrest, mitochondrial membrane potential, and apoptosis showing the combined effect of free MET+TPT and various LB-MSN formulations in MDA-MB-231 cell lines. Cell cycle arrest and mitochondrial membrane potential were performed after 24 h treatment and apoptosis was performed at 48 h with free drugs (MET and TPT) and LB-MSN formulations alone and in combinations. In combination experiments, 200×10^{-6} M of MET and 1×10^{-6} M TPT were used. All results were obtained in triplicate ($n = 3$).

near-infrared (NIR)-labeled (DiR740)LB-MSNs, after achieving the 200–300 mm^3 tumor size (**Figure 5**A). IVIS imaging was obtained prior to and following IV injection of 1 mg kg^{-1} equivalent, DiR-labeled LB-MSNs at the designated time points. Robust fluorescence intensity was observed at the tumor sites within 4 h of LB-MSN injection, following which the signal was sustained for at least 24 h. This was also confirmed by ex vivo imaging of the tumors and major organs collected from the animals, following sacrifice 24 h postinjection (Figure 5A1,A2). In addition to abundant particle uptake at the tumor site, the liver and spleen were also major sites of particle distribution. Little signaling was obtained in the lung and kidney.

2.3.2. Pharmacokinetics and Tumor Distribution

To determine the effect of HIP on pharmacokinetics and tumor distribution of MET and TPT, we have compared coloaded particles with and without trapping agent after i.v. administration. Tumor-bearing mice were injected with MET+TPT

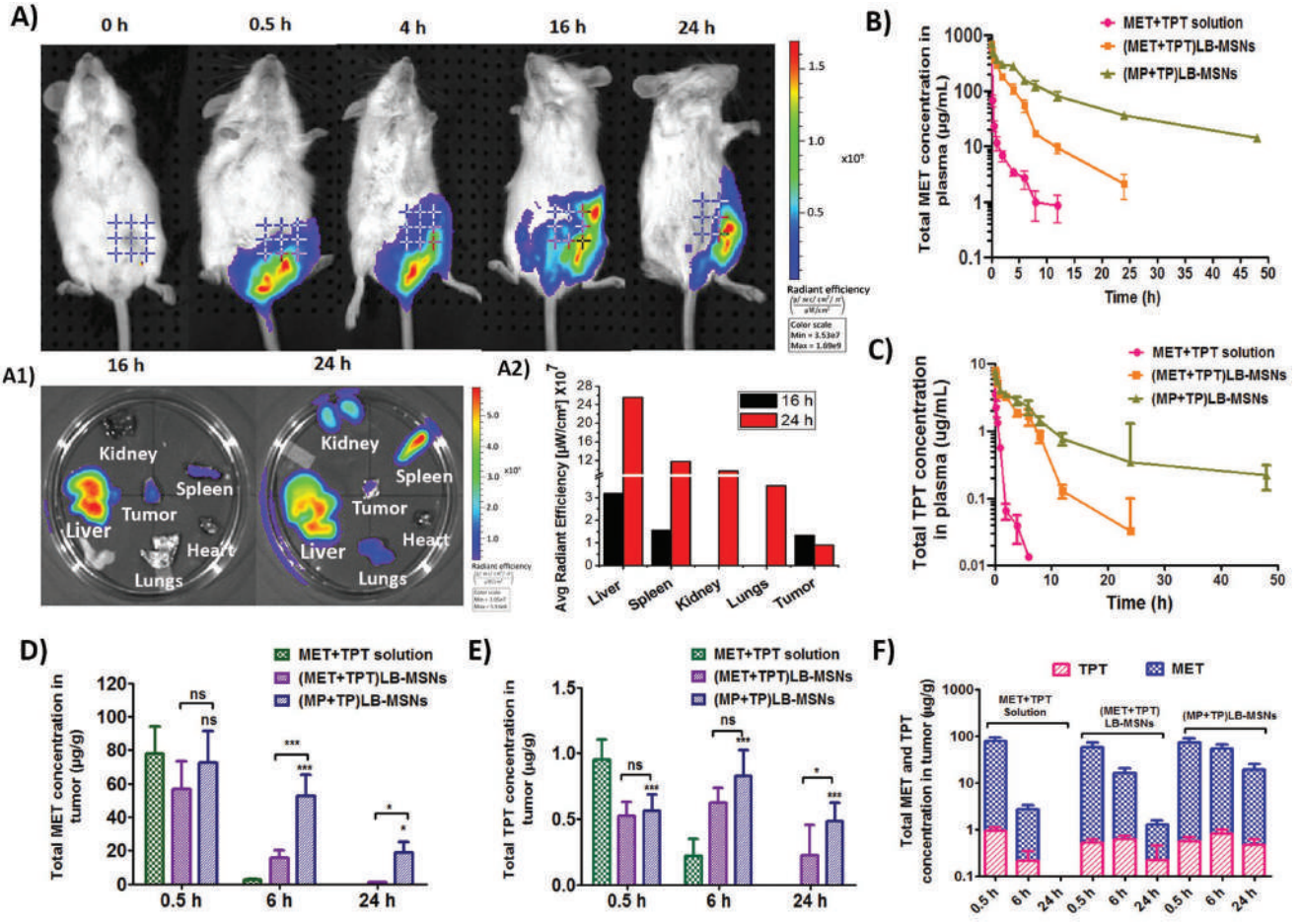

G)

Molar ratio of MET and TPT at the tumor site over 24 h

Time (h)	Molar ratio of MET: TPT at tumor site		
	MET+TPT solution	(MET+TPT)LB-MSNs	(MP+TP)LB-MSNs
0.5	289.51±38.56	386.16±54.23	454.58±53.96
6	40.25±17.30	88.42±14.28	226.88±44.31
24	NA	16.69±4.08	138.91±53.92

Figure 5. A) Representative IVIS images over 24 h to compare the biodistribution of i.v. injected DiR-labeled LB-MSNs to the 4T1 tumor-bearing mice and A1) ex vivo biodistribution of explanted organs in the same experiment; animals were sacrificed after 16 h and 24 h. A2) Comparative radiant efficiency in different organs of interest. B,C) MET and TPT concentrations in plasma of different coloaded LB-MSNs with and without trapping agent (MET and TPT were given a dose of 50 and 1 mg kg^{-1}, respectively). D) Total MET concentration, E) total TPT concentration in tumor tissue with respect to time, all data are expressed as mean ± SD ($n = 3$), statistical significance was determined with one-way ANOVA and differences between groups were determined by Tukey's multiple comparison test, $*p \leq 0.05$; $**p \leq 0.01$; $***p \leq 0.001$; ns, nonsignificant. F) Comparison of total MET and TPT tumor accumulation between the MET+TPT solution and different LB-MSN formulations. G) Molar ratio of MET and TPT at tumor site as free or LB-MSN formulations.

Table 1. Pharmacokinetic parameters of MET and TPT in mice plasma after single intravenous administration of coloaded MET and TPT formulations at a dosage of 50 mg kg^{-1} MET and 1 mg kg^{-1} TPT. Significance level: ***$p \leq 0.001$; **$p \leq 0.01$; *$p \leq 0.05$; ns, nonsignificant versus MET+TPT solution, all data are expressed as mean ± SD ($n = 3$).

	Metformin (MET)			Topotecan (TPT)		
	MET+TPT solution	(MET+TPT)LB-MSNs	(MP+TP)LB-MSNs	MET+TPT solution	(MET+TPT)LB-MSNs	(MP+TP)LB-MSNs
C_{max} [μg mL^{-1}]	542.61 ± 17.84	707 ± 25.45	681.76 ± 134.64	3.60 ± 0.028	7.92 ± 0.073	7.74 ± 0.063
$t_{1/2}$ [h]	3.34 ± 1.37	5.84 ± 1.202^{ns}	14.42 ± 2.58***	1.76 ± 0.028	2.97 ± 0.11***	10.90 ± 0.733***
AUC_{0-t} [μg h mL^{-1}]	694.8 ± 734.63	1355.66 ± 74.24^{ns}	3887.73 ± 340.22***	2.21 ± 0.89	23.120 ± 3.09***	42.063 ± 0.591***
V_{ss} [mL]	155.70 ± 16.5	128.17 ± 14.24	175.59 ± 1.21	6.75 ± 0.19	3.32 ± 0.013	6.25 ± 0.022
Cl [mL h^{-1}]	158.29 ± 3.5	36.33 ± 2.29***	11.99 ± 1.16***	8.88 ± 0.12	0.859 ± 0.0061***	0.430 ± 0.0038***
MRT [h]	1.92 ± 1.79	3.54 ± 0.61^{ns}	14.67 ± 0.87***	0.75 ± 0.04	3.87 ± 0.22***	14.52 ± 0.62***

solution, (MET+TPT)LB-MSNs, and (MP+TP)LB-MSNs through tail vein at an equivalent dose of 50 mg kg^{-1} MET and 1 mg kg^{-1} TPT. Plasma distribution profiles over 48 h are shown in Figure 5B,C, and pharmacokinetic parameters are summarized in **Table 1**. MET+TPT solution eliminated rapidly from the systemic circulation, whereas coloaded MSNs with trapping agent, (MP+TP)LB-MSNs exhibited 2.8-fold, 5.6-fold increase in area under curve $(AUC)_{0-\alpha}$ of MET and 1.8-fold and 19-fold increase in $AUC_{0-\alpha}$ of TPT compared to (MET+TPT)LB-MSNs and MET+TPT solution, respectively. The average half-life of (MP+TP)LB-MSNs was 2.4-fold and 4.3-fold longer for MET and 3.6-fold and 6.7-fold longer for TPT compared to the formulation without trapping agent and drug solutions, respectively. These results indicate longer residence of drug in the body by HIP-based coloaded MSNs which further helps in promoting tumor site accumulation by enhanced permeation and retention (EPR) effect. The lower mean residence time (MRT) and half-life of the MET+TPT solution might be attributed to the rapid distribution of the free drug to organs and rapid elimination. Further, a significant difference between the pharmacokinetic parameters of (MP+TP)LB-MSNs and (MET+TPT)LB-MSNs might be due to the faster release of drugs from the MSNs without trapping agent. Increased $AUC_{0-\alpha}$, MRT, and $t_{1/2}$ values of (MP+TP)MSNs claim the controlled release effect of HIP and long circulation due to lipid bilayer coating.

A comparative tumor distribution study was also performed to assess the tumor localization of the formulations. Figure 5D,E compares the MET and TPT concentrations in the tumor at a different time resulting due to various formulations. Apparently, (MP+TP)LB-MSNs delivered more MET and TPT than MET+TPT solution and (MET+TPT)LB-MSNs. To prove the in vivo synergistic efficacy, it is always necessary to deliver the drug ratios exhibiting synergistic cytotoxicity.[15c] To confirm the delivery of synergistic ratio, we have determined the MET:TPT ratio at the tumor site (Figure 5F). The coloaded formulation with trapping agent, (MP+TP)LB-MSNs had maintained molar ratios of MET to TPT at 138.9 to 454.5 at the end of 24 h, which absolutely fall under the region of synergy determined in in vitro synergy modeling experiments. In contrast, MET+TPT solution reached the tumor at synergistic molar ratios in early time points with no detectable limits at 24 h. Further comparison between formulations with and without trapping agent showed low molar ratios of MET to TPT from (MET+TPT)LB-MSNs, ranging from 16 to 386, clearly demonstrating that HIP-based controlled release of MET and TPT helps in maintaining high tumor site concentrations for a prolonged period of time (Figure 5G).

2.3.3. In Vivo Tumor Regression Studies

After having superior in vitro activity and improved pharmacokinetics, various LB-MSNs were tested for in vivo efficacy in BALB/c mice bearing 4T1 mammary tumors and compared with free MET, TPT, and control. Treatment was started when the tumor volume reached ≈100 mm^3 in all the animals. Each group received i.v. dose of MET and TPT equivalent to 50 and 1 mg kg^{-1}, respectively, on days 1, 4, 8, 12, and 16. The tumor volume versus time curve and tumor photographs are presented in **Figure 6**A,D. Tumor volume was measured throughout the study, and animals were sacrificed on the 20th day of the study started, to harvest the tumors and organs. As shown in Figure 6A, for single drug formulations, both (MP)LB-MSNs and (TP)LB-MSNs had slightly better antitumor activity than the corresponding drug solutions, but no significant difference was observed ($p > 0.05$). For combination formulations, the tumor growth was better inhibited than single drug-loaded formulations. The mixture of solutions (MET+TPT solution) and a mixture of single drug loaded MSNs (MP)LB-MSNs+(TP)LB-MSNs had similar effects. Coloaded (MP+TP)LB-MSNs showed superior antitumor activity than their solutions and the mixture of single drug loaded LB-MSNs with significant differences ($p \leq 0.05$). The final tumor volume at the end of 20 days post-treatment of coloaded (MP+TP)LB-MSNs treated group was 13.9-fold, 4.06-fold, and 1.84-fold lower than control, free MET+TPT, and mixture (MP)LB-MSN+(TP) LB-MSN-treated groups, respectively. Whereas, mixture of LB-MSNs had shown 7.5-fold and 2.20-fold lower tumor volumes compared to control and free MET+TPT groups, respectively. The final tumor weight of coloaded formulation at the end of tumor regression study was 32-fold, 9.69-fold, and 2.29-fold lower than the control group, MET+TPT solution, and mixture(MP)LB-MSN+(TP)LB-MSN group ($p < 0.001$) (Figure 6B). The body weight of mice was also recorded to evaluate the safety of the formulations. As seen in Figure 6C, TPT solution and (TP)LB-MSNs showed

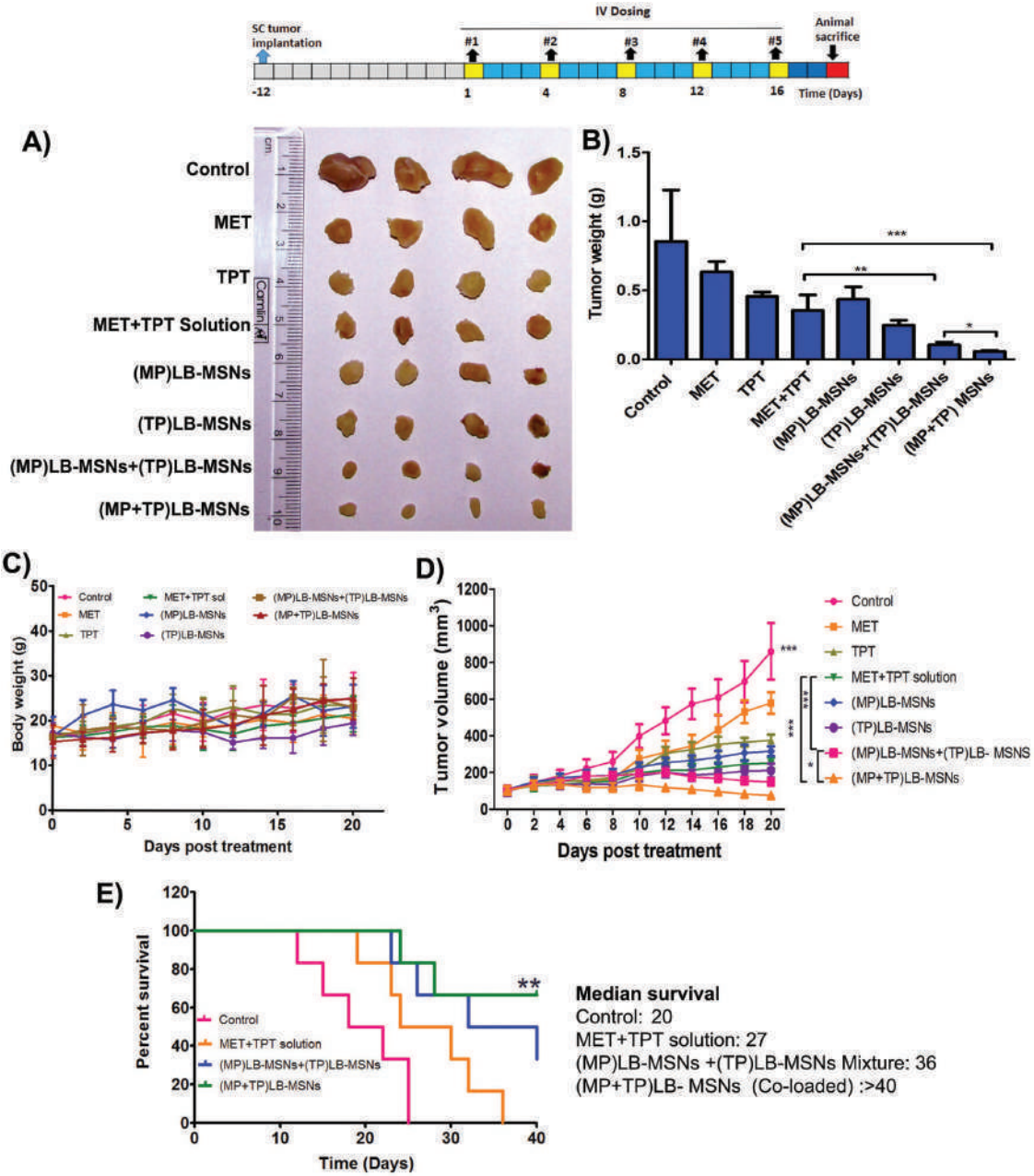

Figure 6. In vivo antitumor activity against 4T1 cells transplanted mammary tumor in female BALB/c mice (MET dose: 50 mg kg^{-1} and TPT dose: 1 mg kg^{-1} body weight). A) Morphology of the tumors harvested at the end of the study. B) Tumor volume versus time at different time points of the study. All data are expressed as mean ± SD ($n = 6$), statistical significance was determined with one-way ANOVA analysis. Differences between groups were determined by a Tukey's multiple comparison test, $*p \leq 0.05$; $**p \leq 0.01$; $***p \leq 0.001$; ns, nonsignificant. C) Body weight changes during the study period. D) Survival rates of 4T1 tumor-bearing mice administrated with a MET+TPT solution and MET+TPT-loaded LB-MSNs, survival data were generated by the Kaplan–Meier method, median survival and statistical significance were determined by log-rank test and Mann–Whitney *U* test, respectively ($n = 6$), $**p \leq 0.01$.

comparative weight loss than free MET and its combination treatment arms MET+TPT solution, (MP)LB-MSNs+(TP) LB-MSNs, and coloaded (MP+TP)LB-MSNs, indicating that MET increasing the safety profile of the TPT. The better tumor inhibition efficacy of coloaded formulations can be attributed to better pharmacokinetic profile and controlled drug delivery with the ratiometric synergistic combinatorial delivery of MET and TPT which resulted in higher residence time in body compared to free drug solution that was getting rapidly eliminating from the body.

2.3.4. Survival Analysis

The survival studies were performed for 40 days after the treatment started, and it was found that survival rates

increased significantly on the administration of coloaded LB-MSNs in comparison to the MET+TPT solution and mixture LB-MSNs. The median survival times for mice treated with saline, MET+TPT solution, mixture of (MP)LB-MSNs+(TP) LB-MSNs, and coloaded (MP+TP)LB-MSNs were 20, 27, 36, and >40 days, respectively (Figure 6E). Treatment with MET+TPT solution and mixture LB-MSNs showed slightly improved survival profiles, whereas coloaded (MP+TP)LB-MSNs enhanced median survival time more than 40 days ($p \leq 0.01$).

3. Conclusion

In this study, we successfully developed a novel in situ HIP-based active loading technique for the efficient loading and controlled release of MET and TPT using pseudo-cell-like LB-MSNs as templates. The developed delivery system was able to control the release of MET and TPT. This resulted in significantly increased intracellular concentrations of MET which is a major translational concern in the MET therapy in cancer. By rational design of these LB-coated MSNs with the synergistic ratio of intended drugs identified by synergy modeling provides deterministic delivery of drug inside the tumor cells. Co-loaded MET and TPT formulations demonstrated higher in vitro cytotoxicity and related apoptotic effects compared to the mixture of single drugs and drug-loaded MSNs. The enhanced tumor efficacy was consistent with the in vitro cell cycle and apoptotic effects. All these presented results prove that translational challenges of MET could be successfully addressed by rational design of the high payload bearing MSNs with controlled release profile. Since the safety and clinical benefits are already proven with other chemotherapeutic agents, therapies could be designed by appropriate selection and delivery of the synergistic ratios at the tumor site. To the best of our knowledge, the present reported active loading procedure using LB-MSNs is the first of its kind and this could be a novel platform technology for the ionic drugs which are difficult to load by using conventional active loading techniques.

4. Experimental Section

Materials: MET was procured from Sigma-Aldrich (St. Louis, MO, USA), TPT HCl was received as a gift sample from Dabur Pharmaceuticals Pvt. Ltd. DSPE-PEG_{2000}, soya phosphatidylcholine, cholesterol, cetyltrimethylammonium bromide (CTAB), Pluronic F-127 were purchased from Sigma-Aldrich (St. Louis, MO, USA). Tetraethylorthosilicate (TEOS), and pamoic acid disodium salt were purchased from TCI chemicals, India Pvt. Ltd. Cell culture media and supplements were purchased from Invitrogen (Carlsbad, CA). MTT, FITC, PI, and RNase were purchased from Sigma-Aldrich (St Louis, MO, USA). High performance liquid chromatography (HPLC) solvents such as acetonitrile and methanol were purchased from Merck (India). All other chemical reagents were of analytical, cell culture grade and obtained from commercial sources. Triple-distilled water (TDW) was prepared from Milli Q system (Millipore, Bedford, MA, USA).

Identification of Synergy between MET and TPT: Before formulation development, the synergy between MET and TPT was screened by using regular cytotoxicity assay (MTT assay). To identify the synergy combinations, 6 × 6 checkerboard format was used, and results were evaluated using COMBENEFIT software package. The detailed procedure of MTT assay and modeling is discussed in cell culture section provided in the Supporting Information.

Selection of APIs and Counterion for HIP Formation: Based on the acid dissociation constants (pK_a) of MET, 12.4, and TPT, 8 and 9.83, PA was evaluated as the counterion for the HIP formation. The detailed procedure of HIP synthesis and evaluation is provided in the Supporting Information.

Preparation of LB-MSNs and Drug Loading by Using the HIP Approach—Loading of Pamoic Acid into MSNs and Lipid Bilayer Coating (PA)LB MSNs: Typical MSN cores were prepared by well-reported Stöbers process[33] (see the Supporting Information for detailed procedure). PA-loaded MSN cores were prepared by passive adsorption process. Briefly, 100 mg of plain MSNs were soaked in 5 mL of aqueous 10×10^{-3} M solution of PA (disodium salt) followed by probe sonication for 2 min with a power output of 20 W. After sonication, MSN suspension was incubated in the same solution for 12 h. The PA-loaded particles were then coated with a lipid film obtained by solvent evaporation of a mixture of 25 mg of SoyPC/Chol/DSPE-PEG_{2000} (molar ratio 7:2.75:0.25) dissolved in chloroform to a 25 mL round bottom flask under rotary evaporation. For uniform coating of the lipid film, probe sonication was used for 10 min with intermittent on/off cycles at a power output of 25 W. Unentrapped PA was removed by centrifugation at 12 000 rpm for 15 min.

Preparation of LB-MSNs and Drug Loading by Using the HIP Approach—Use of (PA)LB MSNs for Remote Loading of MET and TPT: Different conditions were used for the active loading of MET and TPT. MET at a concentration of 10 mg mL^{-1} was dissolved in phosphate buffered sucrose (10% w/v sucrose and phosphate buffered saline (PBS) pH 9), which was mixed with (PA)LB-MSNs to achieve a MET/MSN weight ratio of 1:1. Similarly, TPT at 1 mg mL^{-1} was dissolved in PBS and was mixed with (PA)LB-MSNs to achieve TPT/MSN ratio of 1:2. After that, the mixture was incubated for 4 h at 60 °C under constant shaking. Similar conditions were followed for coloading of both MET and TPT. The ratio of MET and TPT was adjusted based on the percent of entrapment of individual drugs. After incubation, drug-loaded particles were centrifuged at 10 000 rpm for 15 min, and the supernatant was removed and replaced with 10% sucrose for the lyophilization. Lyophilization was carried out at −55 °C for 24 h under 0.1 bar vacuum. For comparative evaluation, formulations without trapping agent were prepared using passive adsorption process and the rest of the procedure was same.

Preparation of LB-MSNs and Drug Loading by Using the HIP Approach—Physicochemical Characterization of LB-MSNs: All developed formulations were evaluated for particle size, zeta potential, drug loading efficiency, in vitro drug release profiles, and confirmation of in situ HIP formation. Apart from that, various parameters that affect the drug loading conditions like, pH, type of gradient ion, and temperature were also evaluated. To confirm the membrane permeability of metformin, in vitro permeability assay was also performed. Detailed methods are described in the Supporting Information.

Preparation of LB-MSNs and Drug Loading by Using the HIP Approach—In Vitro Cell-Based Assays: To evaluate the efficiency of developed formulation, cell-based assays were performed in MDA-MB-231 and 4T1 (human and mouse, respectively) breast cancer cell lines by following established experimental protocols. Cytotoxicity assays and synergy calculations were performed by modeling approach using COMBENEFIT software package in 6 × 6 checkerboard format. Other cell-based assays like cell cycle arrest, apoptosis, mitochondrial membrane potential, cell uptake studies were performed as per the manufacturer and reported experimental protocols. A detailed description of experimental procedures and conditions is provided in the Supporting Information.

Preparation of LB-MSNs and Drug Loading by Using the HIP Approach—In Vivo Studies: All the animals for in vivo experiments were procured from the National Laboratory Animal Center (NLAC) CDRI and acclimatized for 1 week. All the protocols for animal experiments were

approved by the Institutional Animal Ethical Committee CSIR–CDRI (approval no: IAEC/2016/159).

Preparation of LB-MSNs and Drug Loading by Using the HIP Approach—Tumor Model Development: Subcutaneous murine breast cancer model was used for the evaluation of the developed formulations. The breast cancer model was developed in 6–8 week old female BALB/c mice weighing 20–22 g using murine mammary carcinoma cells, 4T1. Cells at a density of 1×10^6 were injected subcutaneously at the mammary gland near to lower right quadrant of the abdomen of mice. In vivo NIRF imaging, pharmacokinetics, and tumor distribution studies were carried out in mice with a tumor volume ranging 200–300 mm^3, whereas tumor regression study and survival analysis were performed in mice with 100 mm^3 tumor volume.

Preparation of LB-MSNs and Drug Loading by Using the HIP Approach—In Vivo NIRF Imaging: In order to observe the biodistribution of the LB-MSNs intuitively, real-time NIRF imaging was applied to monitor the fate of the LB-MSNs in vivo. DiR, a NIRF dye, was selected as an indicator and MSNs were prepared by passive loading approach similar to the procedure followed for the preparation of dye-loaded MSNs in cell uptake studies. 150 µL of (DiR)LB-MSNs containing DiR dose of 1 mg kg^{-1} was injected intravenously via tail vein to 4T1 tumor-bearing female BALB/c mice. After 0.5, 4, 16, and 24 h, mice were anesthetized with 2% isoflurane and placed on their back into a light-tight chamber. At the end of the imaging, the mice were sacrificed and heart, liver, spleen, lung, kidney, and tumor were harvested for ex vivo imaging. The real-time NIRF images were taken using Xenogen IVIS Lumina system (Caliper Life Sciences, USA) with the indocyanine green (ICG) filter (excitation at 745 nm, emission at 835 nm) at time points. The exposure time was set to 3 s. Results were analyzed using Living Image 3.1 software (Caliper Life Sciences, USA).

Preparation of LB-MSNs and Drug Loading by Using the HIP Approach—Pharmacokinetics and Tumor Distribution of MET and TPT from Various Formulations: In order to evaluate the in vivo codelivery of MET and TPT MSNs and the effect of ion trapping agent on the release and distribution, 4T1 tumor-bearing female BALB/c mice were used and they were compared with plain drugs. When tumor volume reached 200–300 mm^3, mice were assigned into 3 groups, 1) free MET+TPT solution, 2) coloaded (MET+TPT)LB-MSNs, without trapping agent, 3) coloaded (MP+TP)LB-MSNs, with trapping agent containing MET and TPT equivalent to 50 and 1 mg kg^{-1}, respectively. At designated time points, mice were anesthetized, blood was collected, plasma separated by centrifugation, and stored at −20 °C until analysis. Tumors were collected and frozen immediately and stored at −80 °C. After extraction from the biological samples, MET and TPT were analyzed by HPLC method as described and plasma concentration–time profiles were fitted to the noncompartmental analysis using Pheonix software package.

Preparation of LB-MSNs and Drug Loading by Using the HIP Approach—In Vivo Antitumor Efficacy: In vivo antitumor efficacy of the MET- and TPT-loaded MSNs was evaluated in 4T1 cells bearing mouse model. When the tumor size reached ≈100 mm^3, mice were randomly divided into eight groups ($n = 5$) and administered through i.v. route with saline, MET solution, TPT Solution, MET+TPT solution, (MP)LB-MSNs, (TP) LB-MSNs, (MP)LB-MSN+(TP)LB-MSN mixture, and coloaded (MP+TP) MSNs, respectively, through tail vein on days 0, 4, 8, 12, and 16. The dosage of MET or TPT was kept at 50 and 1 mg kg^{-1}, respectively. Tumor volumes were measured throughout the experiment and calculated according to the formula: $(L \times W^2)/2$, in which L is the longest and W is the shortest tumor diameter (mm). Mice were sacrificed, and tumors were harvested at the completion of the experiment. Changes in body weights were also measured regularly as the indicator of general toxicity. After completion of experiment tumors was excised, tumor weights were measured and tissues were collected for histology.[27a]

Preparation of LB-MSNs and Drug Loading by Using the HIP Approach—Survival Analysis: In a separate experiment similar to the tumor regression study, 4T1 tumor-bearing mice were divided into four groups with six animals in each group (control, MET+TPT solution, (MP)LB-MSN+(TP)LB-MSN mixture, and coloaded (MP+TP)LB-MSNs and treatment was started after reaching the tumor volume 100 mm^3. Animals were treated as per the protocol described above in the tumor regression study. However, survival study was conducted up to 40 days after the treatment started and end point of survival was defined as animal death or when implanted tumor volume reaches ≈1000 mm^3.

Preparation of LB-MSNs and Drug Loading by Using the HIP Approach—Statistical Analysis: Cell viability and synergy calculations were calculated using three biological replicates. Cell viability and cell growth were normalized to the negative control (untreated cells that receive saline). Synergy calculations and statistical significance were determined using COMBENEFIT software.

In pharmacokinetic studies, statistical significance of tumor distribution data was determined by using one way analysis of variance (ANOVA) in Graphpad prism (GraphPad 5.0 Software, Inc., La Jolla, CA, USA). All data were expressed as mean ± standard deviation (SD) ($n = 3$). Differences between groups were determined by Tukey's multiple comparison test. Asterisks denote statistically significant differences ($^*p < 0.05$; $^{**}p < 0.01$; $^{***}p < 0.001$).

In in vivo tumor regression studies, statistical significance of tumor volume and tumor weight were evaluated by using one way ANOVA in Graphpad prism (GraphPad 5.0 Software, Inc., La Jolla, CA, USA). All data were expressed as mean ± standard deviation ($n = 6$). Differences between groups were determined by Tukey's multiple comparison test. Asterisks denote statistically significant differences ($^*p < 0.05$; $^{**}p < 0.01$; $^{***}p < 0.001$).

Survival data were generated by the Kaplan–Meier method, median survival and statistical significance were determined by log-rank test and Mann–Whitney U test, respectively. All data were expressed as mean ± standard deviation ($n = 6$). The statistical analysis of data was carried out using Graph pad prism 5.0 software (GraphPad PRISM, San Diego, CA, USA). Asterisks denote statistically significant differences ($^*p < 0.05$; $^{**}p < 0.01$; $^{***}p < 0.001$).

Supporting Information

Supporting information is available from the Wiley online library or from the author.

Acknowledgements

The authors would like to thank CSIR, New Delhi for providing research fellowship and the CSIR–CDRI for research facilities. The authors also would like to thank A. L. Vishwakarma and Madhu Chaturvedi for assisting with flow cytometry experiments. And, Dr. Kavita Singh is thankfully acknowledged for contribution in the CLSM facility of Electron microscopy Division. The authors are thankful to the DBT India, for funding through Grant No. GAP0220 and the CSIR–CDRI for funding through Grant No. ESC0103. CDRI communication number for this manuscript was 9724.

Conflict of Interest

The authors declare no conflict of interest.

Keywords

breast cancer, codelivery, ion pairing, mesoporous silica nanoparticles, synergy

Received: March 23, 2018
Revised: July 17, 2018
Published online:

[1] a) A. Kreso, C. A. O'Brien, P. van Galen, O. I. Gan, F. Notta, A. M. Brown, K. Ng, J. Ma, E. Wienholds, C. Dunant, A. Pollett, S. Gallinger, J. McPherson, C. G. Mullighan, D. Shibata, J. E. Dick, *Science* **2013**, *339*, 543; b) R. X. Zhang, H. L. Wong, H. Y. Xue, J. Y. Eoh, X. Y. Wu, *J. Controlled Release* **2016**, *240*, 489.

[2] a) C. E. Ashley, E. C. Carnes, G. K. Phillips, D. Padilla, P. N. Durfee, P. A. Brown, T. N. Hanna, J. Liu, B. Phillips, M. B. Carter, N. J. Carroll, X. Jiang, D. R. Dunphy, C. L. Willman, D. N. Petsev, D. G. Evans, A. N. Parikh, B. Chackerian, W. Wharton, D. S. Peabody, C. J. Brinker, *Nat. Mater.* **2011**, *10*, 389; b) Y. Chen, H. Chen, J. Shi, *Mol. Pharmaceutics* **2014**, *11*, 2495.

[3] a) A. Makkouk, G. J. Weiner, *Cancer Res.* **2015**, *75*, 5; b) T. Yin, L. Wang, L. Yin, J. Zhou, M. Huo, *Biomaterials* **2015**, *61*, 10; c) K. M. Au, Y. Min, X. Tian, L. Zhang, V. Perello, J. M. Caster, A. Z. Wang, *ACS Nano* **2015**, *9*, 8976.

[4] a) L. M. Phan, S.-C. J. Yeung, M.-H. Lee, *Cancer Biol. Med.* **2014**, *11*, 1; b) D. Hanahan, R. A. Weinberg, *Cell* **2011**, *144*, 646; c) G. J. Yoshida, *J. Exp. Clin. Cancer Res.* **2015**, *34*, 111; d) M. A. Pierotti, F. Berrino, M. Gariboldi, C. Melani, A. Mogavero, T. Negri, P. Pasanisi, S. Pilotti, *Oncogene* **2013**, *32*, 1475.

[5] a) Y. K. Chae, A. Arya, M.-K. Malecek, D. S. Shin, B. Carneiro, S. Chandra, J. Kaplan, A. Kalyan, J. K. Altman, L. Platanias, F. Giles, *Oncotarget* **2016**, *7*, 40767; b) I. N. Alimova, B. Liu, Z. Fan, S. M. Edgerton, T. Dillon, S. E. Lind, A. D. Thor, *Cell Cycle* **2009**, *8*, 909; c) A. Sonnenblick, D. Agbor-Tarh, I. Bradbury, S. Di Cosimo, H. A. Azim, D. Fumagalli, S. Sarp, A. C. Wolff, M. Andersson, J. Kroep, T. Cufer, S. D. Simon, P. Salman, M. Toi, L. Harris, J. Gralow, M. Keane, A. Moreno-Aspitia, M. Piccart-Gebhart, E. de Azambuja, *J. Clin. Oncol.* **2017**, *35*, 1421.

[6] G. Zhou, R. Myers, Y. Li, Y. Chen, X. Shen, J. Fenyk-Melody, M. Wu, J. Ventre, T. Doebber, N. Fujii, N. Musi, M. F. Hirshman, L. J. Goodyear, D. E. Moller, *J. Clin. Invest.* **2001**, *108*, 1167.

[7] a) D. R. Morales, A. D. Morris, *Annu. Rev. Med.* **2015**, *66*, 17; b) R. Ramjeesingh, C. Orr, C. S. Bricks, W. M. Hopman, N. Hammad, *Curr. Oncol.* **2016**, *23*, e116.

[8] R. J. Dowling, S. Niraula, V. Stambolic, P. J. Goodwin, *J Mol. Endocrinol.* **2012**, *48*, 12.

[9] M. Peng, K. O. Darko, T. Tao, Y. Huang, Q. Su, C. He, T. Yin, Z. Liu, X. Yang, *Cancer Treat. Rev.* **2017**, *54*, 24.

[10] a) T. Hu, Y. M. Chung, M. Guan, M. Ma, J. Ma, J. S. Berek, M. C. T. Hu, *Sci. Rep.* **2014**, *4*, 5810; b) https://clinicaltrials.gov/ct2/show/NCT01528046, (accessed: March 2018).

[11] J. von Pawel, U. Gatzemeier, J. L. Pujol, L. Moreau, S. Bildat, M. Ranson, G. Richardson, C. Steppert, A. Riviere, I. Camlett, S. Lane, G. Ross, *J. Clin. Oncol.* **2001**, *19*, 1743.

[12] M. Rodriguez, P. G. Rose, *Gynecol. Oncol.* **2001**, *83*, 257.

[13] C. Oberhoff, D. G. Kieback, R. Wurstlein, H. Deertz, J. Sehouli, C. van Soest, J. Hilfrich, M. Mesrogli, G. von Minckwitz, H. J. Staab, A. E. Schindler, *Onkologie* **2001**, *24*, 256.

[14] A. Korfel, C. Oehm, J. von Pawel, U. Keppler, M. Deppermann, S. Kaubitsch, E. Thiel, *Eur. J. Cancer* **2002**, *38*, 1724.

[15] a) L. D. Mayer, T. O. Harasym, P. G. Tardi, N. L. Harasym, C. R. Shew, S. A. Johnstone, E. C. Ramsay, M. B. Bally, A. S. Janoff, *Mol. Cancer Ther.* **2006**, *5*, 1854; b) J. H. Lee, A. Nan, *J. Drug Delivery* **2012**, *2012*, 17; c) R. X. Zhang, P. Cai, T. Zhang, K. Chen, J. Li, J. Cheng, K. S. Pang, H. A. Adissu, A. M. Rauth, X. Y. Wu, *Nanomedicine* **2016**, *12*, 1279.

[16] a) F. Z. Dahmani, Y. Xiao, J. Zhang, Y. Yu, J. Zhou, J. Yao, *Adv. Healthcare Mater.* **2016**, *5*, 1447; b) D. Chen, Q. Tang, J. Zou, X. Yang, W. Huang, Q. Zhang, J. Shao, X. Dong, *Adv. Healthcare Mater.* **2018**, *15*, 201701272.

[17] B. Zhang, T. Wang, S. Yang, Y. Xiao, Y. Song, N. Zhang, S. Garg, *J. Controlled Release* **2016**, *238*, 10.

[18] S. Gadde, *MedChemComm* **2015**, *6*, 1916.

[19] Y. H. Song, E. Shin, H. Wang, J. Nolan, S. Low, D. Parsons, S. Zale, S. Ashton, M. Ashford, M. Ali, D. Thrasher, N. Boylan, G. Troiano, *J. Controlled Release* **2016**, *229*, 106.

[20] Z. Li, J. C. Barnes, A. Bosoy, J. F. Stoddart, J. I. Zink, *Chem. Soc. Rev.* **2012**, *41*, 2590.

[21] a) J. L. Vivero-Escoto, I. I. Slowing, B. G. Trewyn, V. S. Y. Lin, *Small* **2010**, *6*, 1952; b) H. Zhang, D. R. Dunphy, X. Jiang, H. Meng, B. Sun, D. Tarn, M. Xue, X. Wang, S. Lin, Z. Ji, R. Li, F. L. Garcia, J. Yang, M. L. Kirk, T. Xia, J. I. Zink, A. Nel, C. J. Brinker, *J. Am. Chem. Soc.* **2012**, *134*, 15790.

[22] a) K. S. Butler, P. N. Durfee, C. Theron, C. E. Ashley, E. C. Carnes, C. J. Brinker, *Small* **2016**, *12*, 2173; b) Y. He, Z. Su, L. Xue, H. Xu, C. Zhang, *J. Controlled Release* **2016**, *229*, 80; c) W.-H. Chen, G.-F. Luo, Q. Lei, F.-Y. Cao, J.-X. Fan, W.-X. Qiu, H.-Z. Jia, S. Hong, F. Fang, X. Zeng, R.-X. Zhuo, X.-Z. Zhang, *Biomaterials* **2016**, *76*, 87; d) Y. Chen, K. Ai, J. Liu, G. Sun, Q. Yin, L. Lu, *Biomaterials* **2015**, *60*, 111; e) X. Wu, Z. Wang, D. Zhu, S. Zong, L. Yang, Y. Zhong, Y. Cui, *ACS Appl. Mater. Interfaces* **2013**, *5*, 10895; f) P. N. Durfee, Y.-S. Lin, D. R. Dunphy, A. J. Muñiz, K. S. Butler, K. R. Humphrey, A. J. Lokke, J. O. Agola, S. S. Chou, I. M. Chen, W. Wharton, J. L. Townson, C. L. Willman, C. J. Brinker, *ACS Nano* **2016**, *10*, 8325; g) V. Cauda, H. Engelke, A. Sauer, D. Arcizet, C. Bräuchle, J. Rädler, T. Bein, *Nano Lett.* **2010**, *10*, 2484.

[23] Q. Yang, T. Zhang, C. Wang, J. Jiao, J. Li, Y. Deng, *Eur. J. Pharm. Biopharm.* **2014**, *88*, 737.

[24] H. Yu, Q. Wang, Y. Sun, M. Shen, H. Li, Y. Duan, *PLoS One* **2015**, *10*, e0116502.

[25] X. Liu, A. Situ, Y. Kang, K. R. Villabroza, Y. Liao, C. H. Chang, T. Donahue, A. E. Nel, H. Meng, *ACS Nano* **2016**, *10*, 2702.

[26] H. Meng, M. Wang, H. Liu, X. Liu, A. Situ, B. Wu, Z. Ji, C. H. Chang, A. E. Nel, *ACS Nano* **2015**, *9*, 3540.

[27] a) A. Verma, S. Sharma, P. K. Gupta, A. Singh, B. V. Teja, P. Dwivedi, G. K. Gupta, R. Trivedi, P. R. Mishra, *Acta Biomater.* **2016**, *31*, 288; b) S. B. Koh, A. Courtin, R. J. Boyce, R. G. Boyle, F. M. Richards, D. I. Jodrell, *Cancer Res.* **2015**, *75*, 3583.

[28] a) D. M. Jonker, S. A. Visser, P. H. van der Graaf, R. A. Voskuyl, M. Danhof, *Pharmacol. Ther.* **2005**, *106*, 1; b) J. B. Fitzgerald, B. Schoeberl, U. B. Nielsen, P. K. Sorger, *Nat. Chem. Biol.* **2006**, *2*, 458.

[29] M. Jurkiewicz, D. A. Averill-Bates, M. Marion, F. Denizeau, *Biochim. Biophys. Acta, Mol. Cell Res.* **2004**, *1693*, 15.

[30] Y. Feng, C. Ke, Q. Tang, H. Dong, X. Zheng, W. Lin, J. Ke, J. Huang, S. C. Yeung, H. Zhang, *Cell Death Dis.* **2014**, *5*, e1088.

[31] Y. Yu, Z.-H. Wang, L. Zhang, H.-J. Yao, Y. Zhang, R.-J. Li, R.-J. Ju, X.-X. Wang, J. Zhou, N. Li, W.-L. Lu, *Biomaterials* **2012**, *33*, 1808.

[32] X. Cai, X. Hu, X. Tan, W. Cheng, Q. Wang, X. Chen, Y. Guan, C. Chen, X. Jing, *PLoS One* **2015**, *10*, e0133349.

[33] T.-W. Kim, P.-W. Chung, V. S. Y. Lin, *Chem. Mater.* **2010**, *22*, 5093.